Int. J. Electrochem. Sci., 14 **(2019)** 9774 – 9784, doi: 10.20964/2019.10.11

International Journal of ELECTROCHEMICAL SCIENCE
www.electrochemsci.org

Corrosion by Polyaniline/Salicylaldehyde Modified Chitosan in Hydrochloric Acid Solution

Peipei Kong[1,2,*], *Nali Chen*[1,2], *Yong Lu*[1,2], *Huixia Feng*[1,2,*], *Jianhui Qiu*[3]

[1] College of Petrochemical Technology, Lanzhou University of Technology, Lanzhou 730050, China;
[2] State Key Laboratory of Advanced Processing and Recycling of Nonferrous Metals, Lanzhou University of Technology, Lanzhou 730050, China;
[3] Department of Machine Intelligence and Systems Engineering, Faculty of Systems Engineering, Akita Prefectural University, Akita, 015-0055, Japan
[*]E-mail: dongnan_k@163.com; fenghx66@163.com

Received: 20 May 2019 / *Accepted:* 24 July 2019 / *Published:* 30 August 2019

A new type of natural polymer corrosion inhibitor, polyaniline/salicylaldehyde modified chitosan, was synthesized by an innovative method. The inhibition efficiency of polyaniline/salicylaldehyde modified chitosan was evaluated by electrochemical techniques. Surface analysis using SEM characterization were carried out to understand the corrosion inhibition property. Quantum chemical descriptors were investigated to explain the performance of polyaniline/salicylaldehyde modified chitosan as corrosion inhibitor. Experimental results show that the polyaniline/salicylaldehyde modified chitosan had better acid resistance. The quantum chemical study gives insight into the benefits of the corrosion mechanism of polyaniline/salicylaldehyde modified chitosan. It is envisioned that the inhibitor can be used to tailor the properties of the corrosion system for specific applications, resulting in more reliable and durable metal protection in the future.

Keywords: Chitosan; Polyaniline; Corrosion; Inhibition; Quantum chemical

1. INTRODUCTION

While metals have facilitated great progress in modern society, these materials also face tremendous challenges. Among these many challenges, the most important is the corrosion of metal. Various protective measures have been taken to inhibit corrosion in metals. The most direct and effective protection measure is to add corrosion inhibitor. Early inhibitors have gradually fallen out of favour because of the shortcomings and negative environmental impacts of these materials [1-6]. Currently, green and environmentally friendly inhibitors have become popular because it's have high efficiency

and pose no potential harm to the environment or human beings, thus, these materials are favoured by anticorrosion workers [7-15].

Among many green corrosion inhibitors, chitosan and its derivatives have attracted great interest in recent years, not only because chitosan comes from a wide range of sources, but also because its molecular structure contains a lot of active amino and hydroxyl groups. These properties would justify it use as a potential corrosion inhibitor. The corrosion inhibition properties of chitosan and its derivatives have been reported in domestic and foreign literature [16-21]. For example, A.M. Fekry [21] reported that the inhibition efficiency of acetyl thiourea chitosan polymer as corrosion inhibitor for mild steel in 0.5 M H_2SO_4 acid and sulphuric acid. We have made previous efforts to experimentally study the inhibition efficiency of salicylaldehyde modified chitosan and polyaniline/chitosan for corrosion inhibitor on carbon steel in acidic solution [22]. Based on previous work, although our team found that polyaniline synthesized by chemical oxidation polymerization of aniline shows excellent anticorrosive properties in heavy-duty anticorrosive coatings and coatings, the solvent needed for dissolution of polyaniline is special and seriously harmful to the environment. In addition, there are few reports on corrosion inhibitors [23, 24]. Referring to a large amount of literature, although domestic and foreign researchers have studied chitosan and polyaniline corrosion inhibitors, the theoretical research of chitosan and polyaniline corrosion inhibitors is still insufficient. It has not been reported that polyaniline/salicylaldehyde modified chitosan has been used as corrosion inhibitor, and the research on the corrosion inhibition study is not sufficiently thorough.

On the basis of previous work, we have successfully prepared polyaniline (PANI) compounded salicylaldehyde-modified chitosan (Sd-CTS) by a novel method. The inhibition performance of the polyaniline/salicylaldehyde modified chitosan composite (PANI/Sd-CTS) on metal was studied by the electrochemical methods, morphology analysis and quantum chemical calculations. The inhibition mechanism of the PANI/Sd-CTS was preliminarily presented.

2. EXPERIMENTAL

2.1 Materials and inhibitor preparation

All the reagents were analytical grade with no further purification. Aniline (An, analytically pure) were obtained from Aldrich Chemical Co., Ltd. Ammonium persulfate [$(NH_4)_2S_2O_8$, APS] and aminosulfonic acid (NH_2SO_3H) were purchased from Tianjin Daming Chemical Co. Ltd. Chitosan (CTS, medium molecular weight), Salicylaldehyde (Sd) and the Q235 steel were the same as those used in our previous work [22]. The aggressive medium was 1.0 M HCl which was prepared from 37% analytical grade HCl reagent and double-distilled water with or without inhibitor.

2.2 Synthesis of PANI/Sd-CTS composite

First, approximately 0.2 g of CTS was added to 40 mL 0.33 M acetic acid, and 10 mL of Sd was added dropwise to the CTS solution with constant stirring. The mixed solution was heated under reflux

at 60 °C for 6 h. Subsequently, when the Sd-CTS mixed solution was cooled to 10-20 °C, the aniline solution (12 mmol of aniline monomer, 20 mL 0.8 M NH_2SO_3H) was dropped into the salicylaldehyde modified chitosan mixture under slowly stirring. Next, the APS solution was added dropwise to the solution under rapid stirring over a period of 1 h at 0~5 °C. Finally, the reaction was carried out for 6 h at 0~5 °C. The PANI/Sd-CTS precipitated was filtered, washed with distilled water and ethanol then dried under vacuum at 50 °C. The preparing schematic diagram as shown in Fig. 1.

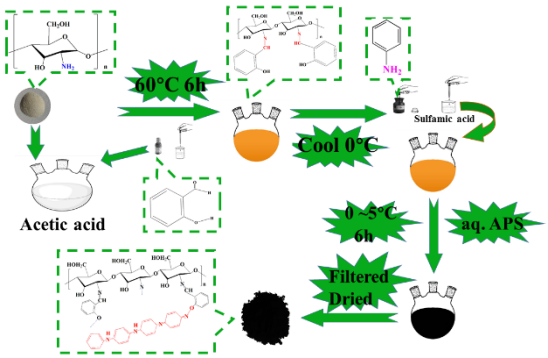

Figure 1. The preparing schematic diagram of PANI/Sd-CTS

2.3 Electrochemical measurements

The electrochemical measurements of the PANI/Sd-CTS were performed by a CHI660E electrochemical workstation. The corrosion cell comprised three electrodes with a platinum sheet (1 cm^2 surface area) as auxiliary electrode and saturated calomel electrode (SCE) as the reference electrode. The Q235 steel, sized 1 cm × 1 cm, was embedded in polytetrafluoroethylene (PTFE) and used as working electrode. The working electrodes were immersed in 100 mL 1.0 M HCl solutions without/with different concentrations of inhibitors (100 ppm, 200 ppm, 300 ppm, 400 ppm) for 1 h. The anodic and cathodic polarization curves were recorded at a scan rate of 1 m/Vs with electrode potential from -0.8 V to 0 V. The inhibition efficiency and corrosion rate were calculated using following equation:

$$C_R = \{(3.286\times10^{-3}) \times (i_{corr}\times M_{Fe})\}/n\,p \quad (1)$$

$$\eta\ \% = (i^0_{corr} - i_{corr})/i^0_{corr}\times100 \quad (2)$$

where (i_{corr}) and (i^0_{corr}) are the corrosion current densities of the uninhibited solution and PANI/Sd-CTS solution. M_{Fe} is the molecular weight of Fe, n is the number of electrons transferred in corrosion reaction, and p is the density of Q235 steel (7.86 g/cm^3).

The electrochemical impedance spectroscopy measurements were performed by changing the frequency from 100 kHz to 0.01 Hz with applying an AC amplitude of 5×10^{-3} V. The inhibition efficiency was calculated using following equation:

$$\eta\ \% = (R_{ct} - R^0_{ct})/R_{ct}\times100 \quad (3)$$

where R^0_{ct} and R_{ct} are the charge transfer resistances in the absence and presence of the inhibitor, respectively.

2.4 Metal surface and inhibitor characterization

The surface morphologies of the films were mainly observed under scanning electron microscopy (SEM, S-4300, Hitachi Co., Ltd. Tokyo, Japan) using electron acceleration between 5 and 10 kV. The structure of the PANI/Sd-CTS was confirmed by Fourier transform infrared spectroscopy (FTIR, JRT-7000; JASCO, Japan).

2.5 Computational methodology

Density functional theory (DFT) was conducted with 6-31G (d, p) basis of Gaussian5.0.9W programme was used to elucidate the chemical reactivity and site selectivity of the molecular systems and to describe the structural nature of the inhibitor regarding corrosion inhibition [25]. The quantum chemical parameters E_{HOMO} (energies of the highest occupied molecular orbital), E_{LUMO} (lowest unoccupied molecular orbital), ΔE (energy gap between E_{LUMO} and E_{HOMO}) and the Mulliken charges on the atoms of the PANI/Sd-CTS molecule was obtained from DFT.

3. RESULTS AND DISCUSSION

3.1 Structure study

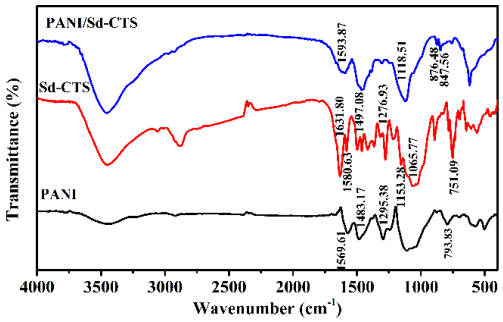

Figure 2. FTIR of PANI, Sd-CTS, PANI/Sd-CTS

The FTIR spectra of PANI, Sd-CTS and PANI/Sd-CTS are shown in Fig. 2. Characteristic peaks at 1596 and 1483, 1295 cm^{-1} are associated with stretching vibrations of C–C, C–N and C=N on quinonoid and benzenoid rings of PANI, respectively [26-28]. In the spectra of Sd-CTS, the strong absorption band at 1631 cm^{-1} is attributed to the C=N vibrations characteristic [29-33]. New absorption peaks appear at 1593, 1118, 876 and 847 cm^{-1}. These results sufficiently confirm the formation of the PANI/Sd-CTS.

3.2 Potentiodynamic polarization measurements

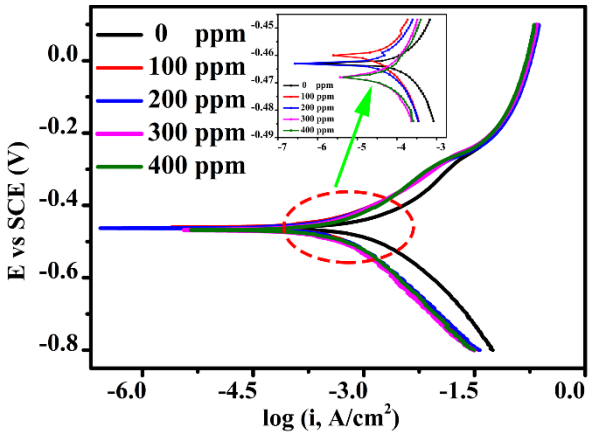

Figure 3. Potentiodynamic polarization curves of Q235 steel in1.0 M HCl containing different concentration of PANI/Sd-CTS at room temperature

The potentiodynamic polarization curves obtained for Q235 in acidic solution without and with various concentration of PANI/Sd-CTS are depicted in Fig. 3. The Tafel parameters, comprised the corrosion potential (E_{corr}) and i_{corr}, obtained from extrapolation the Tafel curves and were listed in Table 1. As should be expected, the i_{corr} for Q235 in PANI/Sd-CTS solution was lower than in pure acid solution. Additionally, the i_{corr} considerably decreased with increasing the concentration of PANI/Sd-CTS, but the η shows the opposite trend. For instance, the η of PANI/Sd-CTS were 0, 69%, 67%, 66%, 545% (see Table 1) as the PANI/Sd-CTS concentration increased from 0 to 400 ppm. These results indicated that the metal surface was covered by PANI/Sd-CTS molecules resulting in the anodic of metal dissolution and cathodic of hydrogen evolution was hindered to a certain extent [34-37]. On the other hand, the η increased as the concentration of PANI/Sd-CTS increased. The reason was that the electronic cloud on PANI/Sd-CTS molecules interacted with the vacant *d* orbitals of iron atoms in the form of donor-acceptor, thus adsorbing PANI/Sd-CTS molecules on metal surface [38-40].

Table 1. Polarization parameters and Q235 steel corrosion inhibition efficiency in 1.0 M HCl containing different concentration of PANI/Sd-CTS at room temperature

Con(ppm)	i_{corr} (A·cm^{-2})	R_P (Ω·cm^2)	E_{corr} (mV vs.SCE)	η %
Blank	1.26×10^{-3}	25	-462	–
100	3.94×10^{-4}	72	-460	69
200	4.21×10^{-4}	67	-463	67
300	4.23×10^{-4}	65	-468	66
400	5.70×10^{-4}	57	-468	55

3.3 Electrochemical impedance spectroscopy

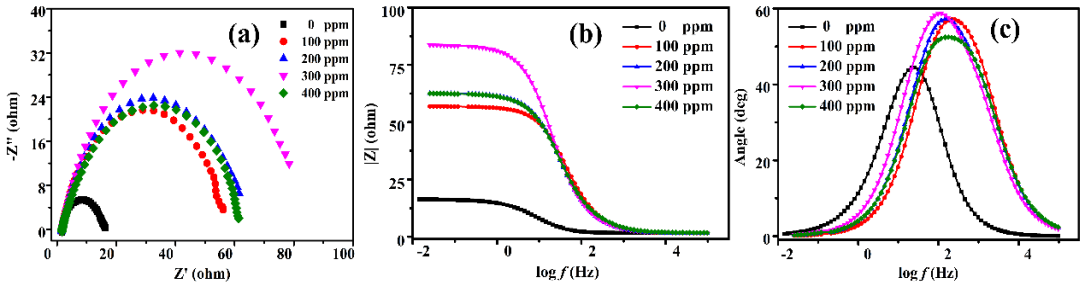

Figure 4. (a) Nyquist, (b) Bode and (c) phase angle plots for Q235 steel in1.0 M HCl containing different concentration of PANI/Sd-CTS at room temperature

Fig. 4 shows the electrochemical impedance results obtained for Q235 steel in various concentration of PANI/Sd-CTS as exemplified in the (a) Nyquist and (b) Bode and (c) phase angle plots representations. As can be seen from the literatures, the Nyquist diagram included a capacitive loop at high frequency and inductive loop at low frequency. The capacitive loop was associated with the charge transfer and double-layer capacitance, while the inductive loop was assigned to the adsorption species or the adsorption-desorption process of inhibitive molecules on the metal surface. Inspection of Fig. 4 (a), shows that the diameter of the capacitive loop increased with increasing PANI/Sd-CTS concentration. This result indicates that the growth up of the inhibiting film on the metal surface interferes with the charge transfer process. Also noteworthy in the Nyquist diagrams, despite the similar appearance of the semicircles, was the plots did not conform to a perfect semicircle. The only reason derived from the inhomogeneity and roughness of the Q235 steel surface [23, 41, 42].

Fig. 4 (b) and (c) present the Bode and phase angle plots of the Q235 carbon steel corrosion in 1.0 M HCl in the absence and presence of PANI/Sd-CTS. Bode plots provided information on the capacitive and resistant behaviour of Q235 steel in 1.0 M HCl containing PANI/Sd-CTS at different frequencies. Phase angle plots revealed one time constant at different concentrations, which is related to the charge transfer process. It is interesting to see that, when the concentrations of PANI/Sd-CTS was 300 ppm, the value of phase angle was maximum. It means that the inhibitor has the greatest protective effect on the Q235 steel surface when the phase angle was maximum [43].

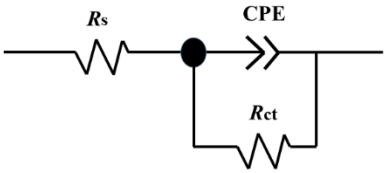

Figure 5. Equivalent circuit used to fit the EIS data for Q235 steel in 1.0 M HCl containing different concentrations of PANI/Sd-CTS at room temperature

The equivalent circuit and fitting parameters of Fig. 5 and Table 2, were derived by using ZSimpWin software to fit the electrochemical impedance results. The proposed circuit comprised the solution resistance (R_s), charge transfer resistance (R_{ct}) and constant phase element (CPE). The CPE was denoted by double layer capacitance (C_{dl}) and was used to compensate for the the surface roughness, inhibitor adsorption, porous layer formation. It was observed that the R_{ct} gradually rose with increasing the concentration of PANI/Sd-CTS and the highest inhibition efficiency concentration was 300 ppm. However, when PANI/Sd-CTS concentration was higher than 300 ppm, the C_{dl} increased, the R_{ct} and the η decreased. This phenomenon may be due to the poor stability of the corrosion products of the PANI/Sd-CTS on Q235 steel surface, where the molecules of PANI/Sd-CTS fall from carbon steel surface under the combined action of anodic dissolution and gravity [44, 45].

Table 2. EIS fitting parameters for Q235 steel in 1.0 M HCl containing different concentration of PANI/Sd-CTS at room temperature

Con (ppm)	R_S ($\Omega\cdot cm^2$)	Y_0 ($s^n\Omega^{-1}\cdot cm^{-2}$)$\times10^{-4}$	n (0<n<1)	$C_{dl}\times10^{-5}$ ($F\cdot cm^{-2}$)	R_{ct} ($\Omega\cdot cm^2$)	η (%)
Blank	1.68	3.93	0.648	9.60	14.38	–
100	1.59	1.98	0.848	4.41	56.19	74
200	1.56	2.50	0.830	2.77	61.70	77
300	1.76	2.76	0.827	2.62	82.74	83
400	1.74	2.70	0.810	7.01	61.56	76

3.4 Surface analysis

Fig. 6 shows the SEM micrographs of the Q235 steel in the (a) abraded state, (b) immersed in 1.0 M HCl, and (c) immersed in 1.0 M HCl +300 ppm PANI/Sd-CTS for 2 h. The Q235 steel in the abraded state seems smooth (a), and exposure to 1.0 M HCl caused serious damage to the surface as evident in the scaly image in (b). In contrast, for (c) 1.0 M HCl +300 ppm PANI/Sd-CTS, the Q235 steel surface was covered with a protective film and the surface was smooth.

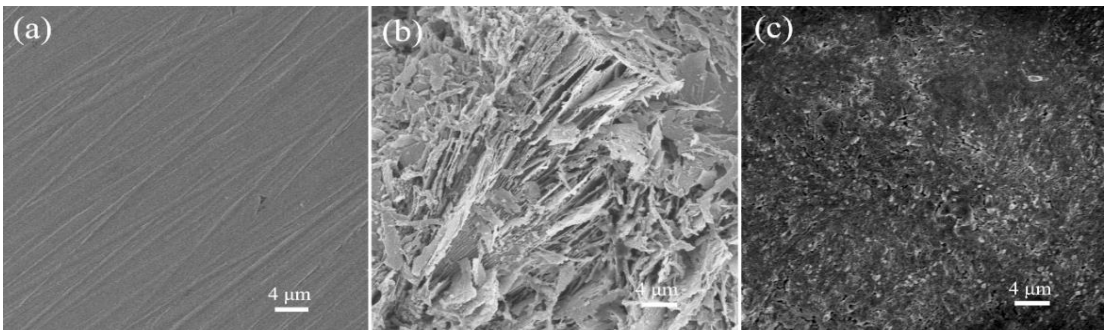

Figure 6. SEM micrographs of (a) the polished Q235 specimen (b) after 2 h of immersion in 1.0 M HCl and (c) after 2 h of immersion in 1.0 M HCl +300 ppm PANI/Sd-CTS at room temperature

3.5 Quantum chemical calculation

Frontier molecular orbital and Mulliken charge analysis were performed to study the reactivity of inhibitor molecule and its various interactions with the metal surface [46]. The structure of the PANI/Sd-CTS monomer was optimized by using DFT at B3LYP/6-31G (d, p) method. The optimized PANI/Sd-CTS monomer structure, HOMO and LUMO are shown in Fig. 7. It was clearly seen that the HOMO mainly located N atoms, C=N groups and benzene ring. As we all known, not only can lone pair of electrons, which contributed by N atoms and C=N groups, chelate with the empty *d* orbitals of the metal, but also the π (or *p*) electrons of the benzene ring interact with the metal surface by sharing electrons with the metal atom [47]. Therefore, the high value of E_{HOMO} was likely to indicate a tendency of the molecule to donate electrons to the appropriate acceptor molecule with low energy and empty molecular orbital.

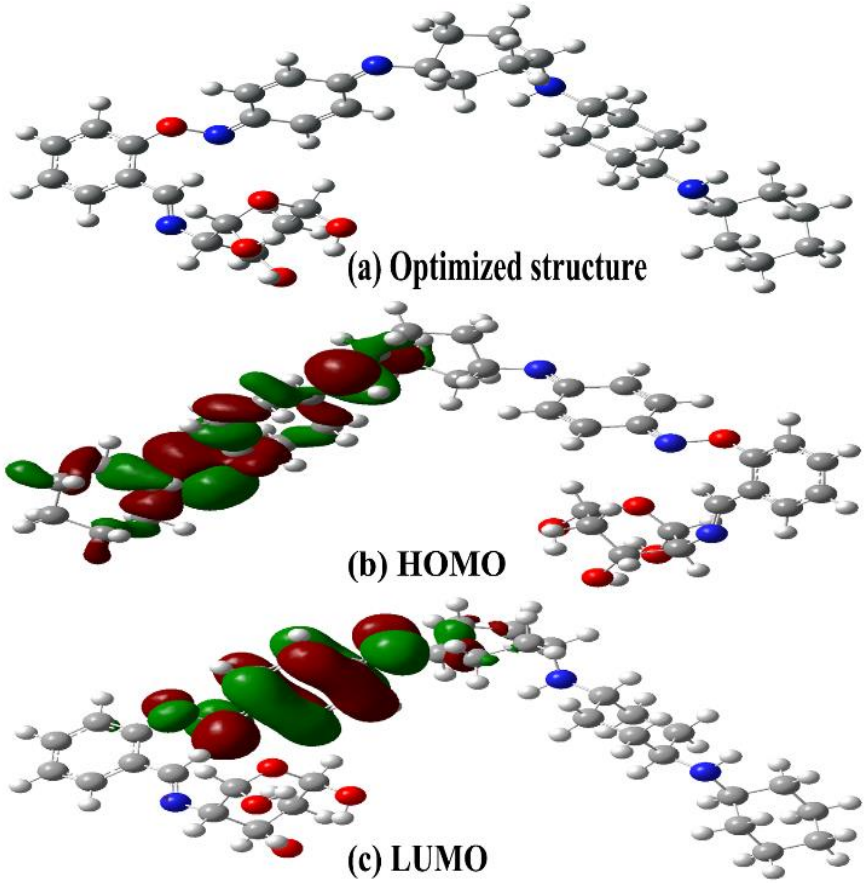

Figure 7. Optimal molecular structure and frontier molecular orbitals (HOMO and LUMO) of PANI/Sd-CTS

The quantum chemical calculations parameters of E_{HOMO} = -5.480 eV, E_{LUMO} = -2.549 eV, a dipole moment of μ = 2.3184 Debye and ΔE ($E_{LUMO} - E_{HOMO}$) = 2.931 eV. According to relevant literatures, the energy of iron occupying the highest molecular orbital $E_{HOMO\ Fe}$= -7.81 eV, the lowest unoccupied molecular orbital $E_{LUMO\ Fe}$= -0.25 eV, and E_{LUMO}-$E_{HOMO\ Fe}$ =5.261 eV > $E_{LUMO\ Fe}$-E_{HOMO} =5.23 eV [48]. It showed that PANI/Sd-CTS molecule provides more electrons than accepts electrons.

In addition, the value of E_{LUMO} indicated its ability of the molecule to accept electrons so that PANI/Sd-CTS had high coordination reactivity on the surface of Q235 steel. In other words, the high inhibition efficiency of a molecule can be attributed to low value of ΔE and the high value of dipole moment. Therefore, PANI/Sd-CTS plays an important role in inhibiting corrosion of Q235 steel in 1.0 M HCl.

4. CONCLUSIONS

We have successfully prepared PANI/Sd-CTS by a novel method. PANI/Sd-CTS was used as corrosion inhibitor for Q235 steel in 1.0 M HCl.

PANI/Sd-CTS was shown to have a good inhibition efficiency against Q235 steel in acidic environment. The electrochemical measurements revealed that PANI/Sd-CTS had a significant effect on Q235 steel in 1.0 M HCl. An increase in the PANI/Sd-CTS concentration increased the inhibition efficiency. Judging from the variation of the inhibition efficiency with the concentration, the metal surface was covered by PANI/Sd-CTS molecules, leading the anodic metal dissolution and cathodic hydrogen evolution to be hindered to a certain extent. The theoretical approach using DFT with the B3LYP/6-31G (d, p) method agreed with the experimental data reported.

ACKNOWLEDGMENTS
This work was supported by the Natural Science Foundation of China (grant numbers: 21664009, 51063003). It acknowledges the computing resources and time of the Supercomputing Center of Cold and Arid Region Environment and Engineering Research Institute of Chinese Academy of Sciences and Supercomputing Environment of Chinese Academy of Sciences.

References

1. A. Pasupathy, S. Nirmala, P. Sakthivel, G. Abirami and M. Raja, *Int. J. Sci. Res. Pub.*, 4 (2014) 1.
2. B.M. Prasanna, B.M. Praveen, N. Hebbar, T.V. Venkatesha, H.C. Tandon and S.B.A. Hamid, *J. Assoc. Arab Univ. Basic Appl. Sci.*, 22 (2015) 62.
3. J. Buchweishaija, *Tanz. J. Sci*., 35 (2009) 77.
4. J. O. Okeniyi, O. A. Omotosho, O. O. Ajayi and C. A. Loto, *Constr. Build. Mater.,* 50 (2014) 448.
5. K. F. Khaled, M. A. Amin, *Corros. Sci.,* 51 (2009) 2098.
6. S. Cheng, S. Chen, T. Liu, X. Chang and Y. Yin, *Mater. Lett*., 61 (2007) 3276.
7. A. Y. I. Rubaye, H. T. Abdulsahib, A. A. Abdulwahid and J. Encapsul, *Adsorp. Sci*., 5 (2015) 155.
8. M. A. Velázquezgonzález, J. G. Gonzalezrodriguez, M. G. Valladarescisneros and I. A. Hermoso-Diaz, *Am. J. Anal. Chem*., 5 (2014) 55.
9. S. A. Umoren, U. M. Eduok, *Carbohydr. Polym*., 140 (2016) 314.
10. M. A. Quraishi, A. Singh, V. K. Singh, D. K. Yadav and A. K. Singh, *Mater. Chem. Phys*., 122 (2010) 114.
11. F. B. Ma, Y. Zhang, H. J. Wang, W. H. Li and B. R. Hou, *Int. J. Electrochem. Sci*., 13 (2018) 235.
12. J. Halambek, K. Berković and J. Vorkapić-Furač, *Corros. Sci*., 52 (2010) 3978.
13. M. Behpour, S. M. Ghoreishi, M. Khayatkashani and N. Soltani, *Mater. Chem. Phys*., 131 (2011) 621.

14. M. M. Solomon, S. A. Umoren, *J. Adhes. Sci. Technol*., 29 (2015) 1060.
15. A. S. Yaro, A. A. Khadom and R. K. Wael, *Alexandria. Eng. J*., 52 (2013) 129.
16. H. Latifa, M. Salah, O. Kafia and K. Abdelhak, *Egypt. J. Petrol*., 22 (2018) 1157.
17. A. Usman, K. M. Zia, M. Zuber, S. Tabasum, S. Rehman and F. Zia, *Int. J. Biol. Macromol*., 86 (2016) 630.
18. N. A. Negm, A. F. El Farargy, A. M. Al Sabagh and N. R. Abdelrahman, *J. Surfactants. Deterg*., 14 (2011) 505.
19. M. M. Solomon, H. Gerengi, T. Kaya, E. Kaya and S. A. Umoren, *Cellul*., 24 (2017) 931.
20. S. A. Umoren, M. J. Banera, T. Alonso-Garcia, C. A. Gervasi and M. V. Mirífico, *Cellul*., 20 (2013) 2529.
21. A. M. Fekry, R. R. Mohamed, *Electrochim. Acta*., 55 (2010) 1933.
22. N. L. Chen, P. P. Kong, H. X. Feng, Y. Y. Wang and D. Z. Bai, *J. Bio. Tribo. Corros*., 5 (2019) 27.
23. F. H. Shi, X. T. Wang, J. Q. Yu and B. R. Hou, *Anti-Corr. Met. Mat*., 58 (2011) 111.
24. Y. Yi, G. Liu, Z. Jin and D. Feng, *Int. J. Electrochem. Sci*., 8 (2013) 3540.
25. Frisch, M. J.; Trucks, G. W.; Schlegel, H. B.; Scuseria, G. E.; Robb, M. A.; Cheeseman, J. R.; Scalmani, G.; Barone, V.; Petersson, G. A.; Nakatsuji, H.; Li, X.; Caricato, M.; Marenich, A.; Bloino, J.; Janesko, B. G.; Gomperts, R.; Mennucci, B.; Hratchian, H. P.; Ortiz, J. V.; Izmaylov, A. F.; Sonnenberg, J. L.; Williams-Young, D.; Ding, F.; Lipparini, F.; Egidi, F.; Goings, J.; Peng, B.; Petrone, A.; Henderson, T.; Ranasinghe, D.; Zakrzewski, V. G.; Gao, J.; Rega, N.; Zheng, G.; Liang, W.; Hada, M.; Ehara, M.; Toyota, K.; Fukuda, R.; Hasegawa, J.; Ishida, M.; Nakajima, T.; Honda, Y.; Kitao, O.; Nakai, H.; Vreven, T.; Throssell, K.; Montgomery, J. A., Jr.; Peralta, J. E.; Ogliaro, F.; Bearpark, M.; Heyd, J. J.; Brothers, E.; Kudin, K. N.; Staroverov, V. N.; Keith, T.; Kobayashi, R.; Normand, J.; Raghavachari, K.; Rendell, A.; Burant, J. C.; Iyengar, S. S.; Tomasi, J.; Cossi, M.; Millam, J. M.; Klene, M.; Adamo, C.; Cammi, R.; Ochterski, J. W.; Martin, R. L.; Morokuma, K.; Farkas, O.; Foresman, J. B.; Fox, D. J. Gaussian 09, revision A.02; Gaussian, Inc.: Wallingford, CT, 2016. 645
26. S. Bhadra, N.K. Singha, D.J. Khastgir, *Appl. Polym. Sci*., 104 (2007) 1900.
27. Y. Wang, M.F. Rubner, *Synth. Met*., 47 (1992) 255.
28. S. M. Imran, Y. N. Kim, G. N. Shao, M. Hussain, Y. H. Choa and H. T. Kim, *J. Mater. Sci*., 49 (2014) 1328.
29. J. T. Wang, Z. R. Lian, H. D. Wang, X. X. Jin and Y. J. Liu, *J. Appl. Polym. Sci*., 123 (2012) 3242.
30. R. Menaka, S. Subhashini, *Polym. Int*., 66 (2017) 349.
31. C. Tengroth, U. Gasslander, F. O. Andersson and S. P. Jacobsson, *Pharm. Dev. Technol*., 10 (2005) 405.
32. T. Tree-Udom, S. P. Wanichwecharungruang, J. Seemork and S. Arayachukeat, *Carbohydr. Polym.,* 86 (2011) 1602.
33. L. S. Guinesi, T. G. Cavalheiro, *Carbohydr. Polym.,* 65 (2016) 557.
34. H. R. Obayes, G. H. Alwan, A. H. M. Alobaidy, A. A. Al-Amiery, A. A. H. Kadhum and A. B. Mohamad, *Chem. Central. J*., 8 (2014) 21.
35. H. Lgaz, R. Salghi, S. Jodeh and B. Hammouti, *J. Mol. Lio.,* 225 (2017) 271.
36. S. K. Saha, P. Banerjee, *Mater. Chem. Front*., 2 (2018) 1674.
37. N. Yilmaz, A. Fitoz, K. C. Emregül, *Corros. Sci*., 111 (2016) 110.
38. P. E. Alvarez, M. V. Fiori-Bimbi, A. Neske, S. A. Brandán, and C. A. Gervasi, *J. Ind. Eng. Chem*., 58 (2018) 92.
39. L. O. Olasunkanmi, I. B. Obot, M. M. Kabanda, and E. E. Ebenso, *J. Phys. Chem. C*., 119 (2015) 16004.
40. U. Eduok, E. Ohaeri, J. Szpunar, *Electrochim. Acta*., 278 (2018) 302.
41. H. Gerengi, M. Mielniczek, G. Gece, M. M. Solomon, *Ind. Eng. Chem. Res*., 55(2016) 9614.
42. C. J. Xing, Z. M. Zhang, L. M. Yu, L. J. Zhang and G. A. Bowmaker, *RSC. Adv*., 4 (2014) 32718.
43. D. Daoud, T. Douadi, S. Issaadi and S. Chafaa, *Corros. Sci*., 79 (2014) 50.

44. G. Fierro, G. M. Ingo, F. Mancia, L. Scoppio and N. Zacchetti, *J. Mater. Sci*., 25 (1990) 1407.
45. R. E. Morsi, E. A. Khamis, A. M. Al-Sabagh, *J. Taiwan. Inst. Chem. Eng*., 63 (2016) 512.
46. H. Xiao, H. Wu, X. Chi, (2009) SCE: Grid Environment for Scientific Computing. In: Vicat-Blance primet P., Kudoh T., Mambretti J. (eds) Networks for Grid Applications. GridNet 2008. Lecture Notes of the Institute for Computer Sciences, Social Informatics and Telecommunications Engineering, vol 2. Springer, Berlin, Heidelberg.
47. Y. J. Qiang, S. T. Zhang, L. Guo, X. W. Zheng, B. Xiang and S. J. Chen, *Corros. Sci*., 119 (2017) 68.
48. S. Q. Hu, J. C. Hu, C. C. Fan, S. Q. Mi, J. Zhang and W. Y. Guo, *Acta. Phys-Chim. Sina*., 26 (2010) 2163.